

An Anomaly Feature-Editing-Based Adversarial Network for Texture Defect Visual Inspection

Hua Yang , Member, IEEE, Qinyuan Zhou, Kaiyou Song , and Zhouping Yin, Member, IEEE

Abstract—Establishing a unified model for the defect inspection of different texture surfaces remains a challenge in the industrial automation field because these surfaces can vary in regular and irregular ways. Current unsupervised learning methods are trained on defect-free samples only and cannot directly address anomalies during testing, which precludes these methods from simultaneously inspecting for various texture defects. In this article, we propose a novel unsupervised anomaly feature-editing-based adversarial network (AFEAN) to accurately inspect various texture defects. To impart the AFEAN with the ability to address anomalies, a paired input, consisting of a defect-free image and an artificially defective image, is utilized for training. First, the AFEAN employs a feature extraction module (FEM) to extract latent features for the paired input. Subsequently, a novel anomaly feature detection module (AFDM) is proposed to detect anomaly features of the artificially defective image in the latent space. In the proposed AFDM, a novel central-constraint-based clustering method is proposed to detect anomaly features by learning the distribution of the latent features. Next, a novel global context feature editing module (GCFEM) is proposed to convert the detected anomaly features to normal features to suppress the reconstruction of defects. Finally, a feature decoding module (FDM) utilizes the edited features to reconstruct the texture background. Through the AFDM and GCFEM, the AFEAN achieves the ability to address anomaly features, effectively suppressing the reconstruction of defects on the texture background. In addition, to further improve the texture reconstruction accuracy, a pixel-level discrimination module (PDM) is employed to reconstruct texture details. In the testing phase, the defects are segmented by the residual image between the input image and the reconstructed texture background. The extensive experimental results demonstrate that the AFEAN achieves the state-of-the-art inspection accuracy.

Manuscript received January 25, 2020; revised April 25, 2020 and July 3, 2020; accepted August 3, 2020. Date of publication August 11, 2020; date of current version November 20, 2020. This work was supported in part by the National Natural Science Foundation of China under Grant 51875228, in part by the project of National Defense Science and Technology Innovation Special Zone under Grant 18-163-11-09-ZD-002-001-14 and Grant 193-A14-202-01-23, and in part by the program for Guangdong Introducing Innovative and Entrepreneurial Teams under Grant 2017ZT07G331. Paper no. TII-20-0350. (Corresponding author: Hua Yang.)

The authors are with the State Key Laboratory of Digital Manufacturing Equipment and Technology, School of Mechanical Science and Engineering, Huazhong University of Science and Technology, Wuhan 430074, China (e-mail: huayang@hust.edu.cn; qinyuanzhou@hust.edu.cn; songkaiyou@hust.edu.cn; yinzhp@mail.hust.edu.cn).

Color versions of one or more of the figures in this article are available online at <https://ieeexplore.ieee.org>.

Digital Object Identifier 10.1109/TII.2020.3015765

Index Terms—Adversarial network, anomaly detection, feature clustering, feature editing, texture defect inspection.

I. INTRODUCTION

TEXTURE surface defects commonly occur in many industrial products, such as fabric [1], steel [2], and thin-film transistor liquid crystal displays (TFT-LCD) [3], due to the complex manufacturing process. These defects are local texture structure destruction, which seriously affects the user experience. To ensure product quality, inspecting for all types of texture defects has become an indispensable part of industrial manufacturing processes.

Visual inspection has been widely applied to automated optical inspection (AOI) [4] equipment to perform automatic texture defect inspection since it is a well-known, noncontact, and flexible technology. However, visual inspection for texture defects remains a challenging task due to different texture backgrounds, scale changes, irregular brightness variations, low contrast, various shapes, and insufficient defective samples. To overcome these challenges, various surface defect inspection methods have been proposed over the past few decades. These methods can be loosely divided into two main categories: traditional methods and deep learning methods.

Traditional methods [5], [6], [7] generally utilize the extracted features to inspect for textural abnormalities. These extracted features are generally handcrafted; thus, they can only address some specific types of texture defect inspection. Aiger and Talbot [6] proposed the phase only transform (PHOT) that only preserves irregular patterns considered to represent defects. Xie and Mirmehdhi [7] proposed the texture exemplars (TEXEMS) method to segment defects on random texture surfaces. Although these traditional methods can segment defects on a specific type of texture image, the performance cannot be sustained simultaneously on various types of texture images because of the handcrafted features.

Deep learning methods have the ability to extract more powerful features by training on different types of texture images. These methods can be categorized as supervised and unsupervised methods according to whether the training data contain labeled defective samples. Supervised methods [8], [9] require large numbers of labeled defective samples to train a model. However, texture surface defects are difficult to collect and label in actual industrial manufacturing, which limits the application of supervised learning methods. In contrast, unsupervised

learning [10], [11] shows great potential for automated online defect inspection in industrial processes, because it requires only readily available defect-free samples. Bergmann *et al.* [11] applied structural similarity to an autoencoder (AE-SSIM) for image background reconstruction to inspect texture defects. However, these unsupervised deep learning methods still cannot achieve good performance for irregular texture surface defects since they are only trained on defect-free samples and cannot directly address anomalies, and they still reconstruct defects on the texture background during testing.

In this article, we propose a novel anomaly feature-editing-based adversarial network (AFEAN) for accurate texture defect inspection. In contrast to general unsupervised learning methods, to impart AFEAN with the ability to directly address anomalies, AFEAN is trained on a paired input that consists of defect-free images and artificially defective images. First, the proposed AFEAN utilizes a feature extraction module (FEM) to extract the latent features. Subsequently, a novel anomaly feature detection module (AFDM) is proposed to detect anomaly features of the artificially defective image in the latent space. Next, a novel global context feature editing module (GCFEM) is proposed for editing the detected anomaly features to normal features to restrain the reconstruction of defects. Finally, a feature decoding module (FDM) is used to reconstruct the edited latent features into texture background. To further improve the reconstruction accuracy, a pixel-level discrimination module (PDM) is employed to make the distribution of the reconstructed pixel-level samples closer to that of the inputs. Thus, by using only defect-free images during training, AFEAN can restrain the reconstruction of defects during testing. The defects are segmented by the residual image between the input image and the reconstructed texture background.

The main contributions of this work are threefold. First, a novel AFEAN is proposed for texture defect inspection, and a series of experimental results demonstrate that it achieves state-of-the-art inspection accuracy. Second, a novel AFDM based on the central constraint clustering method is proposed to detect anomaly features and make the latent features more discriminative. Third, a novel GCFEM is proposed to edit the anomaly features to normal features to remove the defects on the reconstructed texture background.

The remainder of this article is organized as follows. In Section II, the related works regarding texture reconstruction are briefly introduced. In Section III, the proposed AFEAN is elaborated and discussed in detail. Section IV designs extensive experiments to demonstrate the performance of AFEAN. Finally, Section V concludes this article.

II. RELATED WORKS

In this section, we introduce related works on texture reconstruction methods. Texture reconstruction is widely used in the fields of image processing and machine vision, such as visual inspection [11], [12], [13], image style transfer [14], and 3-D reconstruction [15]. Over the past two decades, various methods have been proposed for texture reconstruction, which

fall into two main categories: autoencoder (AE)-based models and generative adversarial networks (GANs).

AE-based models can be used as an unsupervised approach to learn the encoding features in the latent space from input data and then reconstruct the data through them. Hinton and Salakhutdinov first proposed the AE [16] for learning the data representation. Yang *et al.* [13] proposed a multiscale feature-clustering-based fully convolutional AE (MS-FCAE) to reconstruct image backgrounds. These AE-based models minimize the mean absolute error ($L1$) or the squared Euclidean ($L2$) between the original and reconstructed images to train the models and neglect the structural information of images, which causes blurry reconstructed images.

Recently, GANs [17] have shown a promising ability for generating images by a minimax two-player game. However, the original GANs lack a mapping between the input image and the latent features, which makes them only generate images rather than reconstruct images. To address this problem, many methods [18], [19], [20] have been proposed. Makhzani *et al.* proposed an adversarial autoencoder (AAE) [18], which ensures that generating from any part of the prior space results in meaningful samples by matching the aggregated posterior of the latent features with an arbitrary prior distribution. Based on AAE, Pidhorskyi *et al.* [19] utilized an additional adversarial component to improve the image reconstruction quality and improve manifold learning. The discriminator of these GAN-based reconstruction models can be viewed as a more abstract reconstruction loss function, which helps train an encoder-decoder network for reconstructing images with higher quality.

Overall, these texture reconstruction methods are only trained on defect-free samples, and in the testing phase, defects are identified by the residuals of the original and reconstructed images. However, these methods still cannot achieve good performance for irregular texture surface defects since they are only trained on defect-free samples and cannot directly address anomalies during testing. These methods still reconstruct defects on the texture background during testing, which leads to overinspection or misinspection.

In this article, AFEAN is proposed to effectively restrain the reconstruction of defects on the texture background. AFEAN learns to restrain the reconstruction of defects through the novel AFDM and the novel GCFEM by utilizing artificially defective images. Thus, AFEAN can effectively restrain the reconstruction of defects on the texture background, thereby improving the inspection accuracy.

III. PROPOSED AFEAN METHOD

In this section, the proposed AFEAN method is introduced in detail. First, the overall network architecture of AFEAN is introduced. Then, its five modules, including the FEM, AFDM, GCFEM, FDM, and PDM, are presented in detail. Next, the training and inference procedures of AFEAN are introduced. Finally, the parameter setup of AFEAN is discussed.

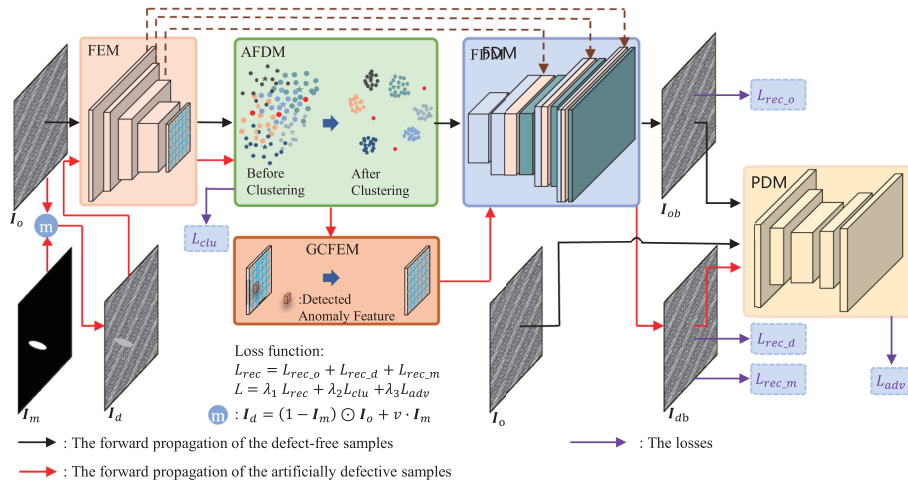


Fig. 1. Overall architecture of the proposed AFEAN method. AFEAN consists of a FEM, an AFDM, a GCFEM, a FDM, and a PDM. During training, the black lines and red lines indicate the forward propagation of the defect-free samples and the artificially defective samples, respectively. The purple lines indicate losses. In PDM, all the layers, including downsampling layers and upsampling layers, adopt a 3×3 convolutional kernel with a stride of 2. The channel numbers of the encoding module increase from 16 to 128 by a multiple of 2. The decoding module is symmetric with the encoding module.

A. Network Architecture of AFEAN

The key point for the inspection of defects in unsupervised methods is to obtain the reconstructed images that have removed the defects of the inputs. Then, the residual image between the reconstructed image and input image is utilized to segment defects. The current unsupervised deep learning models are only trained on defect-free samples and cannot directly address anomalies during testing. Defects are still reconstructed on the texture background during testing, which will eventually lead to overinspection or misinspection. In this study, to accurately inspect various types of texture defects simultaneously, a novel unsupervised AFEAN is proposed.

As shown in Fig. 1, rather than only using defect-free images, AFEAN is trained on a paired input: a defect-free image I_o and its artificially defective image I_d . The artificially defective images are not real defects in production, and they are generated by combining the defect-free images and random masks I_m

$$I_d = (1 - I_m) \odot I_o + \nu I_m \quad (1)$$

where $\nu \in (0, 1)$, \odot denotes the dot product operation, $I_o, I_d, I_m \in R^{W \times H \times C_0}$, and W , H , and C_0 denote the width, height, and channel number of the inputs, respectively. As shown in Fig. 2, the artificially defective images need only to reflect the destruction of the texture. Note that the artificially defective images can simulate most texture surface defects and enable AFEAN to accurately inspect most texture defects. The paired input imparts AFEAN with the ability to address the anomaly features. AFEAN consists of five modules: FEM, AFDM, GCFEM, FDM, and PDM. First, FEM extracts representative features of the paired input, consisting of I_o and I_d . Then, the novel AFDM is proposed to learn the distribution of normal latent features of defect-free images. Feature clustering based on central constraints in AFDM can not only improve the discriminability of encoding features but also achieve the

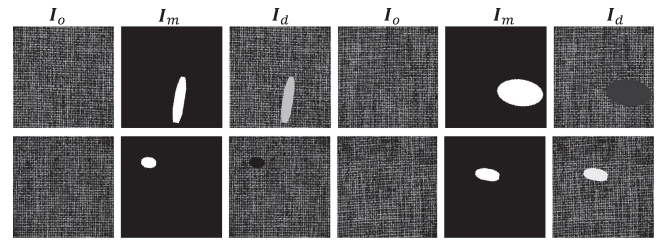


Fig. 2. Examples of artificially defective images. The input images I_o are from the MVTAD [30] dataset.

ability to detect abnormal features. For the detected anomaly features, the novel GCFEM is proposed to edit them to restrain the reconstruction of defects. Finally, FDM utilizes the edited features to reconstruct the texture background of defective images. Through AFDM and GCFEM, the feature input to FDM is normal; therefore, AFEAN can address the anomaly to remove the defects on the texture background. AFEAN is trained in an end-to-end manner under a joint loss function that consists of three losses: texture reconstruction loss, clustering loss, and pixel-level adversarial loss.

Due to the paired input strategy, anomaly feature-editing-based texture reconstruction and pixel-level adversarial learning, AFEAN can restrain the reconstruction of defects and reconstruct accurate texture backgrounds, which is essential for texture defect inspection.

B. Feature Extraction Module and Feature Decoding Module

The FEM and FDM, constituting the basic texture reconstruction module (TRM), are constructed to reconstruct the texture background from the input texture image. The basic TRM is

designed as a deep convolutional neural network with a skip connection, which provides local visual details.

Feature Extraction: In this study, the FEM utilizes five convolutional layers to extract the latent features of the input, where all the sizes of the convolutional kernel are 3×3 except for the last layer. The stride and channel number of the first layer are 1 and C_1 ($C_1=16$ in this study), respectively. Subsequently, three convolutional layers with a stride of 2 increase the channel numbers by a multiple of 2. Finally, the convolutional kernel of the fifth convolution layer is 1×1 with a stride of 1. Thus, FEM extracts the latent features F , where $F \in R^{\frac{W}{8} \times \frac{H}{8} \times C}$, and C is set to 10 in this study.

Feature Decoding: The FDM reconstructs the latent features F into the texture image through several symmetric convolutional layers of the FEM. Similarly, the sizes of all convolutional kernels are 3×3 except for the first layer, which is 1×1 . Similar to the U-net architecture [21], the FDM directly utilizes the features of each layer of the FEM by a skip connection to reconstruct the texture background.

As shown in Fig. 1, TRM takes the texture image I_o or I_d as input and outputs the corresponding texture background I_{ob} or I_{db} , where $I_o, I_d, I_{ob}, I_{db} \in R^{W \times H \times C_0}$. The FEM extracts the latent convolutional features of the input, and then the FDM reconstructs the texture representation into the texture background. The procedure can be formulated as follows:

$$I_{ob} = f_{\theta_T}(I_o) \quad (2)$$

$$I_{db} = f_{\theta_T}(I_d) \quad (3)$$

where $f_{\theta_T}(\cdot)$ denotes the function that combines TRM, AFDM, and GCFEM, and θ_T represents the parameters of FEM, FDM, AFDM, and GCFEM.

C. Anomaly Feature Detection Module

The mainstream unsupervised methods based on deep convolutional neural networks for texture defect inspection [11], [13] are only trained to learn the distribution of the defect-free samples, which causes them to reconstruct defects during the testing procedure. To address this problem, AFDM based on a novel clustering method is proposed to detect abnormal features.

The latent features F from FEM can be viewed as a set of local features, that is, $F=\{f_1, f_2, \dots, f_N\}$, and $f_i \in R^{C \times 1}$, $i \in (1, \dots, \frac{W}{8} \times \frac{H}{8})$. The aim of AFDM is to use K centers and an adaptive threshold T_c to learn the distribution of the latent features, and then those features that are larger than T_c can be viewed as abnormal features. Note that the threshold T_c and K centers are trainable parameters, which are affected only by defect-free images and updated by the clustering loss introduced later. To achieve this goal, the different types of local features in texture images should be separated and clustered into K classes. However, as shown in Fig. 3, the original latent feature distribution of texture images is disordered, which is difficult for clustering [22]. To address this problem, clustering based on central constraints is proposed. Let $C=\{c_1, c_2, \dots, c_K\}$ denote the cluster centers ($c_k \in R^{C \times 1}$). Assuming that all normal latent features are distributed around the corresponding center, the abnormal latent features mapping from the defects will be located

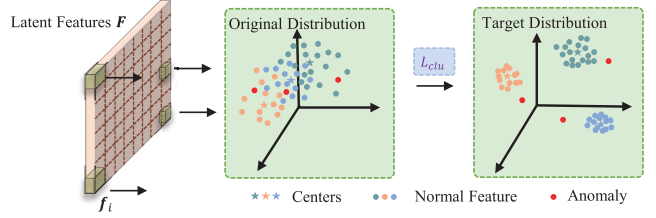


Fig. 3. AFDM schematic. AFDM is used to detect the latent anomaly features. The parameters of AFDM and FEM are updated by L_{clu} to make the original distribution of latent features to the target distribution.

far from the center. The residuals between the latent features and the cluster centers are calculated by

$$R_{ik} = f_i - c_k \quad (4)$$

where $i=1, \dots, N$, $k=1, \dots, K$, and N is the number of latent features. Then, a score is designed to measure the degree to which center each latent feature f_i is normal. That is, the more normal the feature is, the closer it is to the corresponding center. The score is calculated as follows:

$$S_{ik} = \frac{e^{-\alpha_k \|R_{ik}\|^2}}{\sum_{j=1}^K e^{-\alpha_j \|R_{ij}\|^2}} \quad (5)$$

where $\alpha=\{\alpha_1, \dots, \alpha_K\}$ is a set of learned smoothing factors. Note that the smoothing factor controls the magnitude of the distance, and it is updated by the clustering loss introduced later. Each normal latent feature f_i has a distance $d-C$, and the minimum distance indicates to which center the feature belongs

$$d_i = \min_k \|R_{ik}\|^2. \quad (6)$$

The T_c of the central boundary is calculated as follows:

$$T_c = \frac{1}{N} \sum_i d_i + 3\sigma_d \quad (7)$$

where σ_d is the standard deviation of the distances d . Therefore, the latent features whose distance is larger than T_c are viewed as anomalies.

Current deep clustering methods [22], [23], [13] ignore reducing the intraclass variance and increasing the interclass variance, which results in poor clustering performance. To address this issue and accurately detect anomaly features, a novel deep clustering approach based on central constraints is proposed. To make the original distribution tend to the target distribution in Fig. 3, an auxiliary score and a central constraint are proposed.

The auxiliary scores S'_{ik} are proposed to make the distances d more concentrated, which can enhance the discriminability of the latent features. Therefore, the target scores S'_{ik} are calculated by raising S_{ik} to the second power and then normalizing it by the per-center frequency

$$S'_{ik} = \frac{S_{ik}^2 / t_k}{\sum_{j=1}^K S_{ij}^2 / t_j} \quad (8)$$

where $t_k = \sum_{i=1}^N S_{ik}$ is the soft cluster frequency. Following MS-FCAE [13], the Kullback–Leibler (KL) divergence is used

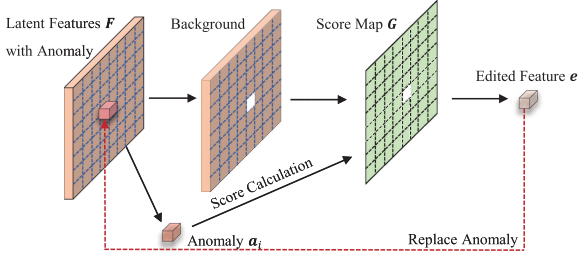


Fig. 4. Architecture of the GCFEM. Each detected abnormal feature can be viewed as a 1×1 convolutional kernel. The matching score is obtained from the convolution between the abnormal feature and the normal background features. Then, the matching score is normalized by the softmax operation to obtain the score map. Subsequently, the corresponding normal feature is obtained by combining the score map and the background features. Finally, the anomaly is replaced by the corresponding edited feature.

to minimize the difference between the distance scores and the auxiliary target scores

$$L_{\text{kl}} = \text{KL}(S' || S) = \sum_{i=1}^N \sum_{k=1}^K S'_{ik} \log \frac{S'_{ik}}{S_{ik}}. \quad (9)$$

MS-FCAE [13] ignores the reduction in the intraclass variance and the increase in the interclass variance. To further reduce intraclass similarity and increase interclass similarity, the following central constraint is proposed:

$$L_c = \frac{\frac{1}{N} \sum_{i=1}^N d_i}{\frac{1}{K^2} \sum_{i=1}^N \sum_{j=1}^K \|c_i - c_j\|^2}. \quad (10)$$

The central constraint L_c can make the FEM module extract more representative latent features by making different centers more dispersive and similar features more compact. As shown in Fig. 3, the distribution of the latent features changes from the original distribution into the target distribution with updating of the parameters by the loss

$$L_{\text{clu}} = L_{\text{kl}} + L_c. \quad (11)$$

Due to the auxiliary score and the central constraint, AFDM makes the same class more compact and different classes more separated. Thus, AFDM can accurately detect anomaly features in the latent space.

D. Global Context Feature Editing Module

Feature editing plays an important role in synthesizing plausible content for missing content in image inpainting. However, current feature editing methods [24], [25], [26] ignore global context information, which leads to a lack of fine textural details in the results. To address this issue, a novel GCFEM is proposed.

For detected anomaly features, editing them to restrain the reconstruction of defects is crucial for texture defect inspection. GCFEM uses the sorted global context information from the normal background features to replace the abnormal features. The background features are sorted according to their similarity with the exception features to be edited and then combined into a new feature for substitution.

As shown in Fig. 4, there is a match score between each detected abnormal feature and each background feature. Cosine

similarity is used to measure the similarity to obtain the match score M

$$M(i, j) = \frac{\langle a_i, b_j \rangle}{\|a_i\| \|b_j\|} \quad (12)$$

where $\langle \cdot \rangle$ denotes the inner product of vectors, $\|\cdot\|$ denotes the modulus length of the vector, and a_i and b_j represent the i th anomaly in F and the j th background feature in F , respectively. Subsequently, the score map G between each detected abnormal feature and the background features is calculated by a softmax operation

$$G_{ij} = \frac{e^{M(i,j)}}{\sum_j e^{M(i,j)}}. \quad (13)$$

In addition, the corresponding normal feature e_i is obtained by combining the score map and the background features and is calculated by the following equation:

$$e_i = \sum_j (G_{ij} \odot b_j). \quad (14)$$

Then, the abnormal feature a_i is replaced by the corresponding normal feature e_i . For all detected anomaly features $A = \{a_1, a_2, \dots, a_n\}$, where n is the number of detected abnormal features, they are processed in the same way as a_i . Finally, the normal latent features after editing the anomaly are used to reconstruct the texture background.

By combining the global context feature information, GCFEM can edit the anomaly features to normal features. Through GCFEM, all the latent features input into FDM are normal, which restrains the reconstruction of defects and is important for accurate texture defect segmentation.

E. Pixel-Level Discrimination Module

Adversarial learning was proposed in [17], and [25], [26] proved that it can improve the reconstruction capability. Here, the PDM is presented, which classifies the real and fake samples at the pixel level.

As shown in Fig. 1, the architecture of the PDM is an encode-decode-like convolutional network. The PDM takes three types of samples as input: the real samples I_o , the reconstructed texture background I_{ob} , and the reconstructed texture background I_{db} , where I_{ob} and I_{db} are treated as fake samples. The output of the PDM is the discrimination score, which predicts the probability that each pixel in the image is from the distribution of the original images to achieve pixel-level discrimination. L_{adv} is denoted as follows

$$\begin{aligned} L_{\text{adv}} = & \frac{1}{W \times H} \sum_{i=1}^W \sum_{j=1}^H \mathbb{E}_{P_{I_o}} [\|\log D_{ij}(I_o)\|_1] \\ & + \frac{1}{W \times H} \sum_{i=1}^W \sum_{j=1}^H \mathbb{E}_{P_{I_{ob}}} [\|\log (1 - D_{ij}(I_{ob}))\|_1] \\ & + \frac{1}{W \times H} \sum_{i=1}^W \sum_{j=1}^H \mathbb{E}_{P_{I_{db}}} [\|\log (1 - D_{ij}(I_{db}))\|_1] \end{aligned} \quad (15)$$

where $\mathbb{E}[\cdot]$ denotes the operation for calculating the expectation and $\|\cdot\|_1$ represents the L_1 norm.

Through adversarial learning based on PDM, the discrepancy between the distribution of the real samples and the fake samples at the pixel level decreases such that the details of texture reconstruction can be further improved.

F. Training and Inference Procedures

To accurately reconstruct texture background images, a multitask loss function consisting of three types of losses is established to optimize the entire AFEAN. The losses include texture reconstruction loss, clustering loss, and pixel-level adversarial loss.

For texture reconstruction, there are three losses: $L_{\text{rec_o}}$, $L_{\text{rec_d}}$, and $L_{\text{rec_m}}$. The loss function aims to minimize the difference between the input image and the reconstructed texture background image by using mean square errors

$$L_{\text{rec_o}} = \mathbb{E}_{P_{I_o}} [\|I_o - I_{ob}\|_2] \quad (16)$$

$$L_{\text{rec_d}} = \mathbb{E}_{P_{I_o}} [\|I_o - I_{db}\|_2] \quad (17)$$

$$L_{\text{rec_m}} = \mathbb{E}_{P_{I_o}} [\beta \|I_m \odot (I_o - I_{db})\|_2] \quad (18)$$

where $\|\cdot\|_2$ represents the L_2 norm. Note that for defective regions, the abovementioned equation is utilized to reconstruct a more detailed textured background, where β is an amplification coefficient $\frac{W \times H}{\text{sum}(I_{\text{mask}})}$, and $\text{sum}(\cdot)$ is a summation operator. Thus, the whole reconstruction loss is as follows:

$$L_{\text{rec}} = L_{\text{rec_o}} + L_{\text{rec_d}} + L_{\text{rec_m}}. \quad (19)$$

To learn the distribution of the defect-free samples and enhance the discriminability of the latent feature, as analyzed in Section III-C, AFDM is trained with clustering loss L_{clu} , which consists of L_{kl} and L_c .

To further improve the texture detail reconstruction, as introduced in Section III-E, (15) is used in pixel-level adversarial learning. Thus, the weighted joint loss is as follows:

$$L = \lambda_1 L_{\text{rec}} + \lambda_2 L_{\text{clu}} + \lambda_3 L_{\text{adv}} \quad (20)$$

where λ_1 , λ_2 , and λ_3 are the weights of the three types of losses.

The entire end-to-end training of AFEAN consists of three procedures. In the first procedure, only FEM and FDM of AFEAN are trained on defect-free images to impart the basic TRM with the ability to extract representative features by optimizing (15) and (16). The second procedure utilizes K centers and a threshold T_c to learn the distribution of the defect-free images, which is optimized by (15), (16), and (11). Finally, the original image, the mask images and the artificially defective images are used as inputs for the third training procedure. By optimizing (20), the AFEAN model achieves the ability to address the anomaly and achieves accurate texture background reconstruction.

After training, the AFEAN model can be employed for texture defect inspection, as shown in Fig. 5, which only uses FEM, AFDM, GCFEM, and FDM. When the defective image is input, the model can edit the anomaly features to restrain the reconstruction of defects. Thus, a corresponding texture background

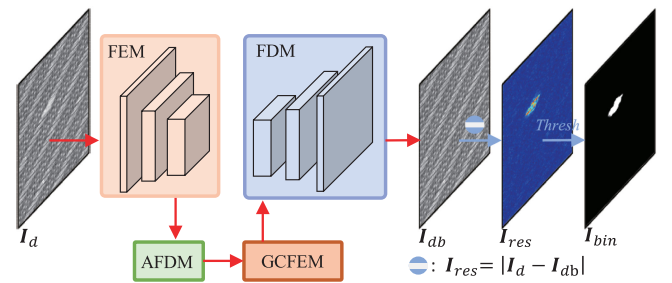


Fig. 5. Network architecture of the inference procedure in AFEAN.

is reconstructed, and the residual image I_{res} between them can be obtained with the following equation:

$$I_{\text{res}} = |I_d - I_{db}|. \quad (21)$$

Subsequently, a median filter operation is applied to the residual images to remove the noise. Finally, a dual-threshold and morphological close operation are applied to the residual images to obtain the resulting binary images I_{bin}

$$I_{\text{bin}}(i, j) = \begin{cases} 0, & \text{if } T_1 < I_{\text{res}}(i, j) < T_2 \\ 1, & \text{otherwise} \end{cases} \quad (22)$$

where $i \in (1, \dots, W)$, $j \in (1, \dots, H)$, and T_1 and T_2 are the two thresholds from I_{res} . The thresholds can be viewed as the boundaries for residual images, where the defects are outside. Assuming that the residuals follow a Gaussian distribution, the two thresholds can be calculated as follows:

$$\begin{aligned} T_1 &= \mu - \varepsilon\sigma \\ T_2 &= \mu + \varepsilon\sigma \end{aligned} \quad (23)$$

where μ and σ are the mean and standard deviation, respectively, calculated from the residual image. ε is adjusted to control the segmentation sensitivity, which is set to 2.5 in this study.

Thus, the trained AFEAN can be used to segment the texture defects with pixel-level accuracy.

G. Parameter Setup

The key hyperparameters of AFEAN include K , λ_1 , λ_2 , and λ_3 .

The number of clusters K influences the learning of the defect-free image distribution, which finally affects the texture background reconstruction accuracy. A K that is too small retains too little texture information and leads to inferior texture background reconstruction accuracy. However, when K is too large, the model has difficulty converging, which influences the performance. Therefore, the recommended range of K is from 8 to 20. In this study, K is set to 16.

λ_1 , λ_2 , and λ_3 are the weights of the three types of losses in (20). In the training procedure, these weights are set to make each loss lie in a range of similar values to balance the influence of each loss. Therefore, in this study, they are set as $\lambda_1 = 1000$, $\lambda_2 = 0.1$, and $\lambda_3 = 1.0$.

TABLE I
TEST DATASETS OF THE TEN TYPES OF TEXTURE SURFACES

Irregular Dataset	Fabric	Tile	Cement	Wallpaper	Wood
Test Image Number	150	150	150	300	60
Regular Dataset	Seat	Cotton	Ceiling	TFT-LCD	Carpet
Test Image Number	150	150	160	168	89

TABLE II
COMPONENT ANALYSIS FOR THE AFEAN ON THE WALLPAPER DATASET

Module	A	B	C	D	E
TRM	✓	✓	✓	✓	✓
Paired input	✓	✓	✓	✓	
AFDM	✓	✓	✓		
GCFEM	✓	✓			
PDM	✓		✓	✓	✓
<i>F1 – Measure</i>	0.852	0.688	0.769	0.719	0.614

IV. EXPERIMENTAL DETAILS

In this section, several sets of experiments are conducted to evaluate the performance of the proposed AFEAN method. Specifically, to illustrate the influence of each component in the AFEAN, a series of analyses for paired input, AFDM, GCFEM, and PDM are conducted. The overall inspection and application performance of AFEAN is qualitatively and quantitatively compared with that of several outstanding methods.

In these experiments, various textural samples are utilized, including regular and irregular textures. The regular textures are seat, cotton, ceiling, TFT-LCD, and carpet. The TFT-LCD samples consist of 2754 defect-free samples and 168 defective samples with a resolution of 256×256 pixels. There are various defects with different sizes and scales on the defective images. The irregular datasets are sourced from DAGM [29] and MV-TAD [30]. **Table I** summarizes the test datasets. All images are resized to 256×256 pixels.

This study adopts the quantitative indicator *F1-measure* to evaluate the performances of these methods

$$F1 - \text{measure} = \frac{2 \times \text{Precision} \times \text{Recall}}{\text{Precision} + \text{Recall}} \quad (24)$$

where $\text{Precision} = \frac{\text{TP}}{\text{TP} + \text{FP}} \times 100\%$, $\text{Recall} = \frac{\text{TP}}{\text{TP} + \text{FN}} \times 100\%$, and TP denotes the number of correctly detected defect pixels in the defect region, FP denotes the number of falsely detected defect pixels in the background region, and FN denotes the number of undetected defect pixels in the defect region. The *F1-measure* indicator is a comprehensive evaluator that utilizes both recall and precision.

A. Ablation Analysis of AFEAN

A series of experiments are conducted on dataset wallpaper [29] to analyze the effect of each component in AFEAN. Note that all the evaluated variants of AFEAN use the same parameter setting to guarantee a fair comparison. The experimental results are shown in **Fig. 6** and **Table II**.

1) *Influence of Paired Input*: Paired input is a novel strategy and the basis of the AFEAN model, making it possible for the

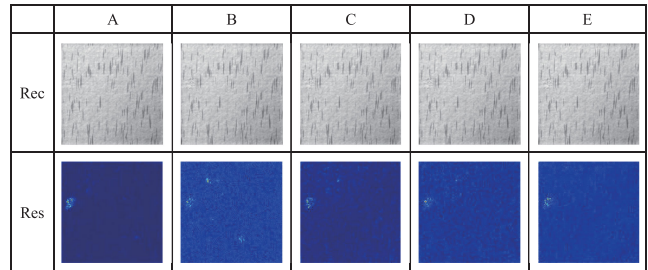


Fig. 6. Examples of images from tests in the ablation experiment. The first row shows the reconstructed images, and the second row shows the residual images. Column A is the result of the whole AFEAN model. Column B is the result of the AFEAN model without the PDM. Column C is the result of the AFEAN model without the GCFEM. Column D is the result of the AFEAN model without paired input. Column E is the result of the AFEAN model without the AFDM.

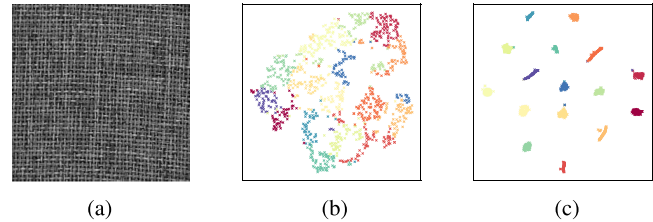


Fig. 7. Influence of clustering in the AFDM. (a) Input image. (b) Distribution of latent features without AFDM. (c) Distribution of latent features with AFDM. (a) Input. (b) Before clustering. (c) After clustering.

model to address the anomaly through the artificially defective image. By combining the random mask and the defect-free image, as shown in (1), the artificially defective image is generated. Thus, they form the paired input.

The experimental results of the ablation of the paired input are described in **Table II**. When the entire paired input is removed, the model can be viewed as a basic TRM composed of an encoder and a decoder. An example of the result is shown in column E of **Fig. 6**. The basic TRM reconstructs the defect during the testing procedure due to training on the defect-free samples only, which leads to misinspection. **Table II** describes that the *F1-Measure* in column E decreases by 0.238 compared to AFEAN (column A).

This experiment demonstrates that the paired input strategy can improve the comprehensive performance. Adding artificially defective images into the training procedure makes it possible for the model to address the anomaly, which benefits the removal of defects.

2) *Influence of AFDM*: AFDM aims to detect the anomaly features in the latent space based on a novel clustering method. The clustering method learns the normal distribution of the latent features and detects the anomaly by an adaptive threshold. Thus, the influence of the clustering method is analyzed in detail.

Column D of **Fig. 6** shows an example of the influence of AFDM. Without the AFDM, the GCFEM is useless. Thus, the defect is reconstructed during the testing procedure, leading to misinspection. In addition, as shown in **Fig. 7**, without the AFDM, the latent feature is tangled, and the AFDM makes

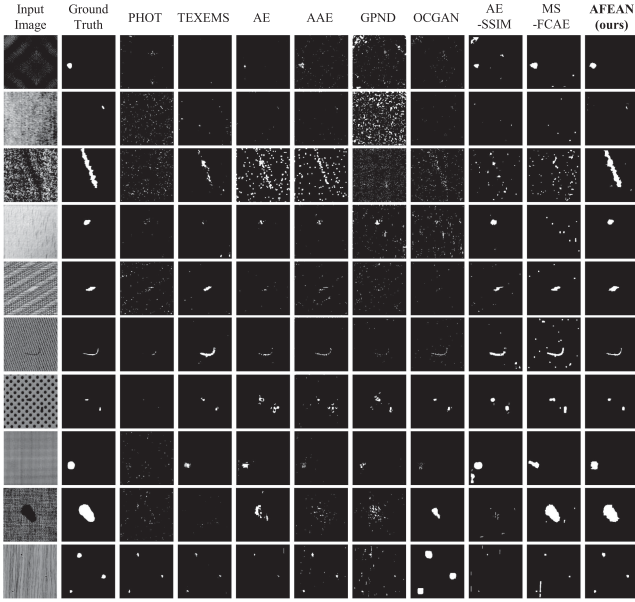


Fig. 8. Examples of the defect inspection performances of the compared methods. From top to bottom are the fabric sample, tile sample, cement sample, wallpaper sample, seat sample, cotton sample, ceiling sample, TFT-LCD sample, carpet sample, and wood sample. (a) Original image. (b) Ground truth. (c) PHOT. (d) TEXEMS. (e) AE. (f) AAE. (g) GPND. (h) OCGAN. (i) AE-SSIM. (j) MS-FCAE. (k) AFEAN.

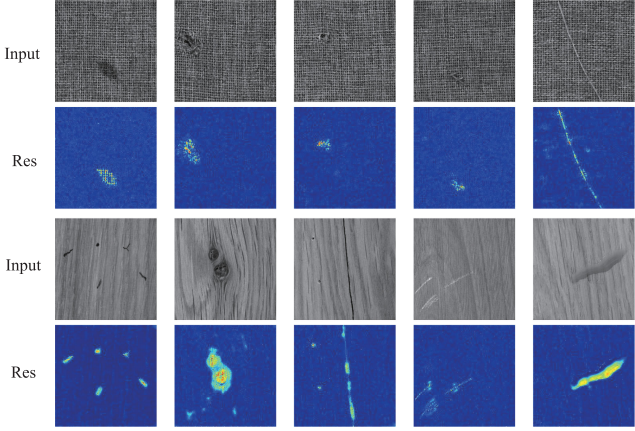


Fig. 9. Examples of the defect inspection performances of AFEAN. The odd rows show the defective images in the test, and the even rows show the corresponding residual images.

different centers more dispersive and similar features more compact. **Table II** lists the experimental results, and the AFEAN (column A) improves the *F1-Measure* by a margin of 0.133 compared to the model without AFDM (column D).

The experiments demonstrate that the AFDM can improve defect inspection due to the central constraint clustering method. The clustering method can learn the distribution of the normal samples and improve the discriminability of the latent features by an auxiliary score. This helps detect the anomaly and reconstruct a more accurate texture background.

3) Influence of GCFEM: GCFEM is proposed to edit the anomaly latent features to suppress the reconstruction of the

TABLE III
F1-MEASURES OF DIFFERENT METHODS ON TEN TYPES OF TEXTURES

Dataset	Fabric	Tile	Cement	Wallpaper	Seat	Cotton	Ceiling	TFT-LCD	Carpet	Wood
PHOT	0.001	0.262	0.011	0.132	0.202	0.273	0.547	0.452	0.106	0.219
TEXEMS	0.001	0.411	0.285	0.142	0.598	0.524	0.436	0.556	0.033	0.238
AE	0.352	0.194	0.217	0.391	0.140	0.407	0.475	0.678	0.088	0.127
AAE	0.401	0.174	0.190	0.333	0.226	0.412	0.564	0.487	0.089	0.264
GPND	0.006	0.032	0.087	0.213	0.167	0.433	0.588	0.583	0.059	0.151
OCGAN	0.001	0.242	0.167	0.085	0.249	0.457	0.761	0.603	0.284	0.373
AE-SSIM	0.219	0.010	0.158	0.513	0.599	0.546	0.655	0.625	0.024	0.100
MS-FCAE	0.727	0.340	0.079	0.112	0.645	0.660	0.630	0.739	0.184	0.222
AFEAN	0.841	0.624	0.734	0.852	0.760	0.753	0.880	0.867	0.513	0.527

The significance of bold entities in table denotes the best F1-Measure among all compared methods.

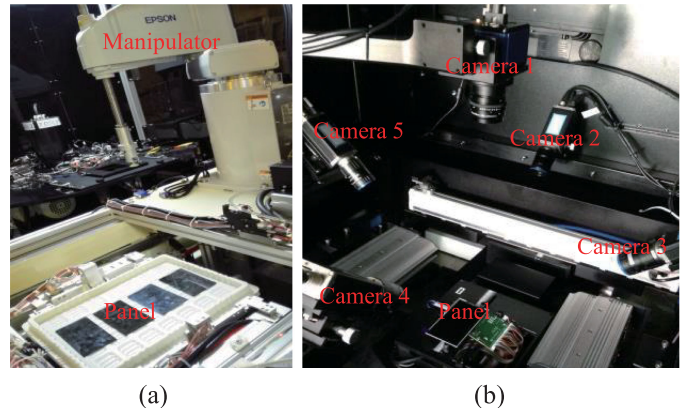


Fig. 10. AOI equipment for TFT-LCD defect inspection. (a) Automatic material delivery module. (b) Automatic optical inspection module.

defects. Without the GCFEM, the AFEAN has no ability to address the detected anomaly.

Column C of **Fig. 6** shows the example of the result of the AFEAN without GCFEM. When GCFEM is removed from AFEAN, the defect is reconstructed during the testing procedure, leading to misinspection. The experimental results are described in **Table II**. AFEAN (column A) improves the *F1-Measure* by a margin of 0.083 compared to the module without GCFEM (column C).

This experiment verifies that editing the anomaly features can improve the performance of defect inspection. By fusing global context features to replace the anomaly features, the model can remove the defects in the image and reconstruct the corresponding texture background, which further improves the *F1-Measure*.

4) Influence of PDM: PDM aims to further improve the texture background accuracy by utilizing a pixel-level adversarial learning mechanism. To verify the effectiveness, we removed the entire PDM from AFEAN.

Column B of **Fig. 6** shows an example of the experimental result. The accuracy of the reconstructed texture background is not good, leading to overinspection and misinspection. The experimental results are listed in **Table II**. Compared to the AFEAN (column A), when the entire PDM (column B) is removed, the *F1-Measure* decreases by 0.164.

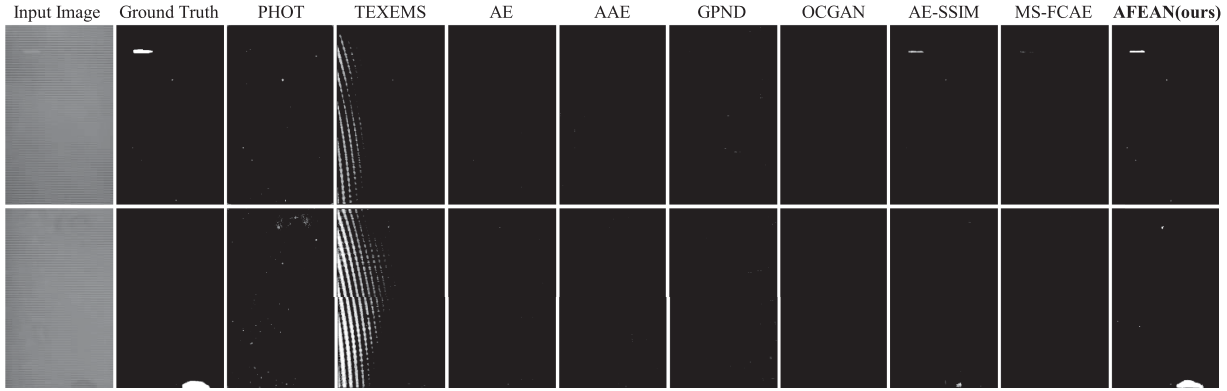


Fig. 11. Examples of TFT-LCD defect inspection results of different methods.

This experiment demonstrates that PDM can improve the accuracy of the texture background because it can learn more elaborate texture details by classifying the real and fake at the pixel level.

B. Overall Performance Comparison

To verify the performance of the proposed AFEAN method, the inspection performance of AFEAN is compared with that of several traditional methods, including PHOT [6] and TEX-EMS [7], and with that of several outstanding unsupervised deep learning methods, including AE [16], AAE [18], GPND [19], OCGAN [20], AE-SSIM [11], and MS-FCAE [13]. For each type of texture surface, AFEAN is trained on a defect-free sample with paired input and is then tested on the test set for this type of texture surface, as described in Table I. As analyzed in Section III-G, the parameter setup is the same for all types of texture surfaces.

Some inspection results of these methods on the ten types of texture samples are shown in Fig. 8. The traditional methods (PHOT and TEXEMS) achieve inferior accuracy for complex texture surfaces, such as the fabric and wallpaper samples in Fig. 8. Thus, these methods cannot inspect all types of texture surface defects due to the handcrafted feature. In contrast, the deep-learning-based methods can learn the texture representation through the convolutional operation regardless of the regular or irregular texture surfaces. However, current deep-learning-based methods (AE, AAE, GPND, OCGAN, AE-SSIM, and MS-FCAE) cannot address the anomaly, leading to inferior inspection accuracy, especially for the tile, cement, and wood samples in Fig. 8. In comparison, AFEAN achieves good performance on all types of defects and texture surfaces. Furthermore, as shown in Fig. 9, AFEAN can also accurately inspect various realistic defective images, such as cuts, holes, scratches, and metal contamination.

The quantitative experimental results are described in Table III. From the comparison of various methods, AFEAN is superior in terms of the *F1-measure*. Compared to the second-best results, AFEAN improves the *F1-measure* value by margins of 0.114, 0.213, 0.449, 0.339, 0.115, 0.093, 0.119, 0.128, 0.229, and 0.154 on the ten types of texture samples. Note that the performance of AFEAN on Cement dataset is greatly improved

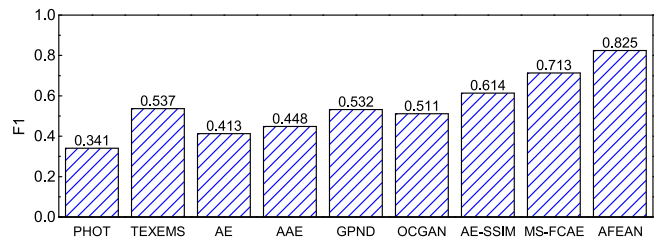


Fig. 12. Inspection results of different methods for 127 defective TFT-LCD images.

because the defects on Cement test dataset are similar to the artificial defects. In addition, the AFEAN can address anomalies to suppress the reconstruction of defects and utilize PDM to reconstruct a more accurate texture background.

These experimental results demonstrate that AFEAN achieves the best performance among all the compared methods on the texture surfaces. The improvement in the inspection accuracy is because AFEAN can address the anomaly to accurately reconstruct the texture background without defects.

C. Application

As shown in Fig. 10, AFEAN is implemented in our AOI equipment for the online inspection of TFT-LCD defects to further evaluate its practical performance. A second TFT-LCD defect dataset that includes 46 defect-free samples and 127 defect samples was collected. These samples have a resolution of 1536×2560 pixels, of which the training dataset cropped from the 46 defect-free samples is utilized to train the model and the 127 defect samples are used for testing. We compare the performance with previously used methods.

Fig. 11 shows some examples of the inspection results. All types of TFT-LCD defects, including spot defects, line defects, and low contrast defects, can be accurately inspected using the proposed approach, whereas the other methods are suitable only for specific defect types. In addition, Fig. 12 shows the *F1-measure* of different methods during defect inspection on the TFT-LCD defect dataset. AFEAN performs better than the other eight methods on the second TFT-LCD defect dataset, and compared with the second-best performance, it improves the *F1-measure* score by a margin of 0.112.

In summary, all the experimental results demonstrate that the proposed AFEAN achieves the best inspection accuracy. The AFEAN method utilizes the AFDM and GCFEM to suppress the reconstruction of the defects, and PDM is used to improve the texture background reconstruction. Thus, AFEAN improves the inspection accuracy for various texture defects.

V. CONCLUSION

In this article, we proposed an unsupervised AFEAN method that was suitable for accurately inspecting various types of texture surface defects. This method was only trained on a paired input and does not require any practical labeled defect samples. The proposed AFEAN utilized FEM to extract convolutional features for textural representation. Then, AFDM based on a clustering method with a central constraint was proposed to detect the anomaly features. To suppress the reconstruction of defects, GCFEM was proposed to replace the anomaly features with a combination of the normal latent features. Thus, FDM utilized the edited features to reconstruct the texture background. Furthermore, to improve the texture reconstruction accuracy, PDM was employed to reconstruct texture details with higher quality. Thus, by using only defect-free images during training, AFEAN can suppress the reconstruction of defects during testing. The extensive experimental results on several typical texture surface datasets demonstrated that the AFEAN method achieved the state-of-the-art inspection accuracy. In follow-up research, we will focus on how to generate more complicated defects that can simulate the internal structure of real defects.

REFERENCES

- [1] K. Zhang, Y. Yan, P. Li, J. Jing, X. Liu, and Z. Wang, "Fabric defect detection using salience metric for color dissimilarity and positional aggregation," *IEEE Access*, vol. 6, pp. 49170–49181, 2018.
- [2] H. Wang, J. Zhang, Y. Tian, and H. Chen, "A simple guidance template-based defect detection method for strip steel surfaces," *IEEE Trans. Ind. Informat.*, vol. 15, no. 5, pp. 2798–2809, May 2019.
- [3] H. Yang, K. Song, S. Mei, and Z. Yin, "An accurate Mura defect vision inspection method using outlier-prejudging-based image background construction and region-gradient-based level set," *IEEE Trans. Autom. Sci. Eng.*, vol. 15, no. 4, pp. 1704–1721, Oct. 2018.
- [4] H. Yang, S. Mei, K. Song, B. Tao, and Z. Yin, "Transfer-learning-based online Mura defect classification," *IEEE Trans. Semicond. Manuf.*, vol. 31, no. 1, pp. 116–123, Feb. 2018.
- [5] W. C. Li and D. M. Tsai, "Defect inspection in low-contrast LCD images using Hough transform-based nonstationary line detection," *IEEE Trans. Ind. Informat.*, vol. 7, no. 1, pp. 136–147, Feb. 2011.
- [6] D. Aiger and H. Talbot, "The phase only transform for unsupervised surface defect detection," *Emerg. Topics Comput. Vis. Appl.*, pp. 215–232, 2012.
- [7] X. Xie and M. Mirmehdi, "Texems: Texture exemplars for defect detection on random textured surfaces," *IEEE Trans. Pattern Anal. Mach. Intell.*, vol. 29, no. 8, pp. 1454–1464, Aug. 2007.
- [8] Y. Li, W. Zhao, and J. Pan, "Deformable patterned fabric defect detection with Fisher criterion-based deep learning," *IEEE Trans. Autom. Sci. Eng.*, vol. 14, no. 2, pp. 1256–1264, Apr. 2017.
- [9] H. Dong, K. Song, Y. He, J. Xu, Y. Yan, and Q. Meng, "PGA-Net: Pyramid feature fusion and global context attention network for automated surface defect detection," *IEEE Trans. Ind. Informat.*, to be published, doi: 10.1109/TII.2019.2958826.
- [10] S. Mei, H. Yang, and Z. Yin, "An unsupervised-learning-based approach for automated defect inspection on textured surfaces," *IEEE Trans. Instrum. Meas.*, vol. 67, no. 6, pp. 1266–1277, Jun. 2018.
- [11] P. Bergmann, S. Löwe, M. Fauser, D. Sattlegger, and C. Steger, "Improving unsupervised defect segmentation by applying structural similarity to autoencoders," in *Proc. 14th Int. Joint Conf. Comput. Vis., Imag. Comput. Graph. Theory Appl.*, 2019, pp. 372–380.
- [12] R. Ren, T. Hung, and K. C. Tan, "A generic deep-learning-based approach for automated surface inspection," *IEEE Trans. Cybern.*, vol. 48, no. 3, pp. 929–940, Mar. 2018.
- [13] H. Yang, Y. Chen, K. Song, and Z. Yin, "Multiscale feature-clustering-based fully convolutional autoencoder for fast accurate visual inspection of texture surface defects," *IEEE Trans. Autom. Sci. Eng.*, vol. 16, no. 3, pp. 1450–1467, Jul. 2019.
- [14] Y. Li, C. Fang, J. Yang, Z. Wang, X. Lu, and M. Yang, "Universal style transfer via feature transforms," in *Proc. Adv. Neural Inf. Process. Syst.*, 2017, pp. 386–396.
- [15] I. Kemelmacher-Shlizerman and R. Basri, "3D face reconstruction from a single image using a single reference face shape," *IEEE Trans. Pattern Anal. Mach. Intell.*, vol. 33, no. 2, pp. 394–405, Feb. 2011.
- [16] G. E. Hinton and R. R. Salakhutdinov, "Reducing the dimensionality of data with neural networks," *Science*, vol. 313, no. 5786, pp. 504–507, 2006.
- [17] I. Goodfellow *et al.*, "Generative adversarial nets," in *Proc. Adv. Neural Inf. Process. Syst.*, 2014, pp. 2672–2680.
- [18] A. Makhzani, J. Shlens, N. Jaitly, I. Goodfellow, and B. Frey, "Adversarial autoencoders," 2015. [Online]. Available: <https://arxiv.org/abs/1511.05644>
- [19] S. Pidhorskyi, R. Almohsen, and G. Doretto, "Generative probabilistic novelty detection with adversarial autoencoders," in *Proc. Adv. Neural Inf. Process. Syst.*, 2018, pp. 6822–6833.
- [20] P. Perera, R. Nallapati, and B. Xiang, "OCGAN: One-class novelty detection using GANs with constrained latent representations," in *Proc. IEEE Conf. Comput. Vis. Pattern Recognit.*, 2019, pp. 2898–2906.
- [21] O. Ronneberger, P. Fischer, and T. Brox, "U-net: Convolutional networks for biomedical image segmentation," in *Proc. Int. Conf. Med. Image Comput. Comput.-Assisted Intervention*, 2015, pp. 234–241.
- [22] E. Min, X. Guo, Q. Liu, G. Zhang, J. Gui, and J. Long, "A survey of clustering with deep learning: From the perspective of network architecture," *IEEE Access*, vol. 6, pp. 39501–39514, 2018.
- [23] J. Xie, R. Girshick, and A. Farhadi, "Unsupervised deep embedding for clustering analysis," in *Proc. Int. Conf. Mach. Learn.*, 2016, pp. 478–487.
- [24] C. Barnes, E. Shechtman, A. Finkelstein, and D. B. Goldman, "Patch-Match: A randomized correspondence algorithm for structural image editing," *ACM Trans. Graph.*, vol. 28, no. 3, p. 24, 2009.
- [25] D. Pathak, P. Krähenbühl, J. Donahue, T. Darrell, and A. A. Efros, "Context encoders: Feature learning by inpainting," in *Proc. IEEE Conf. Comput. Vis. Pattern Recognit.*, 2016, pp. 2536–2544.
- [26] Z. Yan, X. Li, M. Li, W. Zuo, and S. Shan, "Shift-net: Image inpainting via deep feature rearrangement," in *Proc. Eur. Conf. Comput. Vis.*, 2018, pp. 1–17.
- [27] G. Kyberg, "Kyberg texture dataset v. 1.0," Centre for Image Analysis, Swedish University of Agricultural Sciences and Uppsala University, External report (Blue series) No. 35, 2011. [Online]. Available: <http://www.cb.uu.se/~gustaf/texture/>
- [28] P. Mallikarjuna, A. T. Targhi, M. Fritz, E. Hayman, B. Caputo, and J. O. Eklundh, The KTH-tips2 database, Computational Vision and Active Perception Laboratory, KTH Royal Institute of Technology, Stockholm, Sweden, 2006.
- [29] M. Wieler and T. Hahn, "Weakly supervised learning for industrial optical inspection," Jun. 25, 2017. Available: [Online]. <https://hci.iwr.uni-heidelberg.de/node/3616>
- [30] P. Bergmann, M. Fauser, D. Sattlegger, and C. Steger, "MVTec AD—A comprehensive real-world dataset for unsupervised anomaly detection," in *Proc. IEEE Conf. Comput. Vis. Pattern Recognit.*, 2019, pp. 9592–9600.



Hua Yang (Member, IEEE) received the B.S. degree in mechanical design, manufacturing and automation and the M.S. degree in mechatronic engineering from the Huazhong University of Science and Technology, Wuhan, China, in 2006 and 2008, respectively, and the Ph.D. degree in high speed machine vision from Hiroshima University, Higashihiroshima, Japan, in 2011.

He was with Hiroshima University as a Research Associate from 2011 to 2012 and as an Assistant Professor from 2012. He was an Associate Professor from 2013 to 2019 and currently is a Professor with the School of Mechanical Science and Engineering, Huazhong University of Science and Technology. His current research interests include high-speed vision and its applications (object recognition and detection, particle image velocity, and dynamic-based vision inspection).



Qinyuan Zhou received the B.S. degree in mechanical design, manufacturing, and automation from the Huazhong University of Science and Technology, Wuhan, China, in 2018, and the M.S. degree in mechatronic engineering from the State Key Laboratory of Digital Manufacturing Equipment and Technology, Huazhong University of Science and Technology, Wuhan, in 2020.

His current research interests include image segmentation, object detection, and deep learning.



Kaiyou Song received the B.S. degree in mechanical design, manufacturing, and automation from Wuhan University, Wuhan, China, in 2015. He is currently working toward the Ph.D. degree in mechatronic engineering with the State Key Laboratory of Digital Manufacturing Equipment and Technology, Huazhong University of Science and Technology, Wuhan.

His current research interests include image segmentation, object detection, and deep learning.



Zhouping Yin (Member, IEEE) received the B.S., M.S., and Ph.D. degrees in mechanical engineering from the Huazhong University of Science and Technology, Wuhan, China, in 1994, 1996, and 2000, respectively.

He is currently a Professor with the School of Mechanical Science and Engineering, Huazhong University of Science and Technology. Since 2005, he has been the Vice Head of the State Key Laboratory of Digital Manufacturing Equipment and Technology,

Huazhong University of Science and Technology. He is currently leading a research group and conducting research in electronic manufacturing equipment and technology, including flexible electronics, and machine vision.